
Article

CLARA WebGIS: sharing soil and building geophysical data for seismic characterization of the city of Matera (Southern Italy)

Nicola Tragni^{1,2}, Giuseppe Calamita^{1,*}, Lorenzo Lastilla^{3,4}, Valeria Belloni⁵, Roberta Ravanelli⁵, Michele Lupo¹, Vito Salvia¹ and Maria Rosaria Gallipoli¹

¹ National Research Council of Italy (CNR-IMAA), Tito Scalo, Italy

² School of Engineering, University of Basilicata, Potenza, Italy

³ Department of Computer, Control and Management Engineering Antonio Ruberti (DIAG), Sapienza University of Rome, 00185 Rome, Italy

⁴ Sapienza School for Advanced Studies, 00161 Rome, Italy

⁵ Geodesy and Geomatics Division, DICEA, Sapienza University of Rome, 00184 Rome, Italy

* Correspondence: giuseppe.calamita@imaa.cnr.it

Abstract: In the context of seismic risk, studying the characteristics of urban soils and of the built environment means adopting a holistic vision of the city taking a step forward compared to the current microzonation approach. Based on this principle, CLARA WebGIS aims to collect, organise, and disseminate the available information on soils and buildings in the urban area of Matera. The geodatabase is populated with i) 488 downloadable geological, geotechnical, geophysical, surveys; ii) geological, geomorphological, and seismic homogeneous microzones maps and iii) a new Digital Surface Model. The CLARA WebGIS (<https://smartcities-matera-clara.imaa.cnr.it/>) is the first publicly available database reporting for the whole urban area the spatial distribution of the fundamental frequencies for soils and the overlying 4043 buildings, along with probability levels of soil-building resonance. The WebGIS is addressed to a broad target of end users (local government, engineers, and geologists, etc.) as a support to the implementation of seismic risk mitigation strategies in terms of urban planning, seismic retrofitting, and management of post-earthquake crises. We recommend that the database be managed by local administrators, who would also have the task of deciding on future developments and continuous updating as new data becomes available.

Keywords: seismic risk; WebGIS; seismic resilience; HVNSR; fundamental frequency; soil-building resonance level; DSM

1. Introduction

Today we are witnessing an acceleration of the global urbanization phenomenon: it is estimated that in 2050 about 66% of the world population will reside in cities. In Europe, since about 2020, 80% of the population lives in urban areas [1]. Italy is characterized by a large number of medium-sized cities (50,000-200,000 inhabitants) and historical centers of inestimable historical and architectural value highly exposed to catastrophic events (e.g., earthquakes, landslides, volcanic eruptions, etc.) and extreme climatic events. Therefore, with the increase in urbanization there is a significant increase in the demand for smart technologies for the management of interventions related to the security of the territory in urban areas [2,1]. The Sendai Framework for Disaster Risk Reduction (UN 2015) [3] and The Paris Agreement, 2030 Agenda for Sustainable Development [4] contain the main references and criteria for risk reduction and constitute a general framework in which it is essential to include national strategies on risk knowledge, assessment, and prevention. The priority actions defined in the Sendai Framework illustrate the main issues to which national governments must be able to direct research activities: 1) deepen knowledge of risk factors; 2) strengthen governance capacities; 3) investing in risk reduction by

strengthening the resilience of communities and systems, instead of concentrating actions in post-event responses; 4) improve preparation through the implementation of specific and integrated measures. Examples of good practices in the adoption of smart technologies to improve environmental sustainability, mobility and safety of citizens are already present in Europe and Italy in particular [5]. Here administrations have long started strategies for the introduction and pervasive diffusion of digital technologies in urban areas (e.g. smart sensors, IoT, cloud computing), transforming cities into open laboratories and stimulating scientific creativity and technological innovation.

In full coherence with the initiatives already underway at an international level, the CLARA project, promoted by a large public-private partnership, was funded by Italian Ministry of Education, University and Research in the frame of a national call on the topic "Smart Cities & Communities – Thematic Priority: Homeland Security" [6]. The scientific and technological challenge of the "CLARA" project has consisted in developing, from a Smart Cities perspective, innovative products and services for the mitigation of seismic and hydrogeological risks in urban and semi-urban areas through the active involvement of public administrations (service oriented approach). In the framework of this project we have pursued two objectives: i) the development of systemic approach for the characterization of the main physical properties of the urban subsoil and overlying built environment based on the full integration of the most modern, non-invasive, expeditious and low-cost geophysical technologies [7-10]; ii) digital archiving of all geological, geotechnical, geophysical and engineering data for the city of Matera, acquired during the CLARA project and already available. In this sense, a high potential is present in the synergistic use of modern information and communication technologies and in the paradigm of open data. WebGIS is one of the most widely used technologies for the dissemination of open data, for multiple purposes and in varied contexts, such as tourism, archeology, agriculture, environment, etc. [11-15]. Aiming at improving global cooperation and communication with other countries, Shi et al. (2009) [11] designed a WebGIS system to relate the genetic classification of the soils of China with the soil taxonomy. Manna et al. (2020) [12] demonstrate how a geospatial decision support system can assist in the planning and management of olive groves and provide operational support to stakeholders.

The use of WebGIS technologies has also been widespread for natural risk assessment and communication [16-19]. As concerns the geo-hydrological risk theme WebGIS tools have been used for the analysis and/or the management of the risk deriving from floods or landslides [20-22], for slope stability analysis [23] for online mapping of unstable rock slopes [24]. Salvati et al. (2009) [25] designed and shared a WebGIS to disseminate information on historical landslides and floods in central Italy. Even in the field of seismic risk, in which the presented work is inserted, WebGIS and geodatabase technologies have been used for the development of interactive tools for the definition of seismic hazard scenarios and risk analysis [26], for the assessment of seismic damage in the seaport of Gioia Tauro [27] or for choosing the optimal routes in the case of a seismic event [28]. Other authors have published databases to share: acceleration recordings of earthquakes in urban areas of Kalachori (Greece) [29], or the permeability of fault zones and surrounding protolithic rocks in sites around the world [30]. Although some authors have implemented and published software system to store and visualize subsoil data to be used in seismic microzonation [31], to the best of our knowledge no databases or WebGIS tools relating to soil-building interaction in urban areas have currently been made public.

The soil-building resonance effect is a well known and extensively studied phenomenon, which can arise during seismic events when the oscillation frequency of a building is very close to that of the foundation soil causing an increase of damage [32-35]. The soil-building interaction effect for a single/limited number of closed-spaced buildings has been numerically and experimentally studied [36,35,37,38], while for the urban scale as a whole only numerical simulation approaches have been proposed [39,40,33,41-45]. Recently, Agea-Medina et al. (2020) [46] have evaluated the probability of resonance effect in several districts of municipalities of Alicante and Elche while other authors have produced soil-buildings resonance level maps based on numerical relations provided by seismic

regulations [47], Tallini et al. (2020) [48] and on extensive collection of experimental data [8]. As a legislative point of view the microzonation studies focus exclusively on seismotectonic, lithostratigraphic and geotechnical aspects of shallow soil, completely neglecting the presence and role of buildings [8]. Thanks to seismic microzonation studies it is possible to know exactly the areas susceptible to seismic amplification and instabilities, but there is not at all information about areas of cities where the soil - building resonance effect could take place during earthquakes.

In this paper, we present an innovative open tool, with the dual function of geodatabase and disseminative WebGIS, through which it is possible to visualize and download (i) geological, geotechnical, and geophysical data; (ii) the spatial distribution of the main resonance frequency for urban soils; (iii) the main vibrational frequencies for the 4043 overlying buildings; (iv) the spatial distribution of the soil-building resonance levels for the urban area of Matera (<https://smartcities-matera-clara.imaa.cnr.it/>). In addition, users can also rely on a Digital Surface Model (DSM) of the city of Matera and its surroundings, which was generated with a cross-sensor multi-view approach from a triplet of optical satellite images. DSMs, which incorporate the natural ground surfaces, buildings, vegetation, and other objects higher than the underlying topographic surface [49,50], can serve as a valuable input for the characterization of urban structures. In this way, DSMs address the requirement of municipalities for reliable and up-to-date information for land-use and infrastructure planning, for creation and continuation of development plans and overall monitoring of changes [51]. The increasing availability of new high-resolution optical spaceborne sensors allows to produce precise DSMs (such as the one included in the CLARA WebGIS) ensuring low cost, speed of data acquisition and processing, and relaxed logistic requirements [52]. For detailed presentation of the experimental design and the methodology adopted to produce the soil-building resonance map and to generate the DSM, the interested readers can refer to Gallipoli et al. (2020) [8] and to Lastilla et al. (2021) [53], respectively.

2. CLARA WebGIS: data sources

The CLARA WebGIS is populated with two types of data sources: i) open data made available by public institutions and ii) experimental geophysical data about shallow soils and buildings collected both in previous geological studies supporting territorial planning and within the CLARA project. All data was inserted in the GIS environment by means of shapefiles and linked tables and then stored into the CLARA geodatabase. Geological, geophysical, geotechnical, and engineering data are organized in 25 layers with specific vector geometries (Table 1). The queries to the database can be graphically formulated just by using the hand cursor icon, avoiding the need of playing with the SQL language. The available base maps are: OpenStreetMap, Bing Aerial Layer, Bing Road Layer, Bing Hybrid Layer, Google Hybrid, Google Normal, Google Satellite, Ortho Map, Dark Base Map.

Table 1. Characteristics of all objects present in the Web-GIS. Single and double asterisk indicate respectively pre-existing and new geological/geophysical downloadable data.

CLARA	Vector geometry	#	Download
OD Age of construction	point	2648	-
OD Typology	point	2648	-
OD State of conservation	point	2648	-
RSDI Height max	point	4522	-
RSDI edifici is	polygon	11802	-
RSDI unità volumetrica	polygon	25497	-
ISTAT Sassi area	polygon	1	-
ISTAT census variables	polygon	318	-
Calcarenite Sampling Station	point	8	*
Down hole	point	18	*

HVNSR soil	point	117 (10)	**(*)
HVNSR buildings	point	96 (34)	**(*)
MASW	point	8	*
Mechanical Surveys	point	234	*
Seismic Refraction Surveys	point	7	*
Surface features	point	2	-
Geomorphology	polygon	301	-
Geology	polygon	13	-
MOPS	polygon	52	-
Building resonance level	polygon	4043	-
Building frequency	polygon	4043	-
Soil isofrequency map	polygon	7652	-
Soil isoamplitude map	polygon	7652	-
DSM m (Orthometric Heights)	raster	-	-
DSM blg Height	raster	-	-

2.1. Open data

We have used open data from three sources: i) Regional Spatial Data Infrastructure of the Basilicata Region (RSDI) [54], ii) OpenData (OD) Matera [55] iii) Italian National Institute of Statistics (ISTAT) [56]. RSDI (<http://rsdi.regione.basilicata.it/dbgt-ctr/>) is the main channel of the Basilicata Region for disseminating updated territorial information with technical and thematic cartographic production. OD Matera is a catalogue that allows to search, access, download and preview open data relative to the city of Matera through a single access point (<http://dati.comune.matera.it/>). ISTAT is a public research organization producing official statistics operating in interaction with the academic and scientific communities (<https://www.istat.it/en/>). Two shapefiles from RSDI (original names: "edifici_is" and "unità volumetrica"), one from OD Matera portal (original name: rnc_4326.shp) and two from ISTAT (original names: "R17_11_WGS84" and "R17_indicatori_2011_sezioni") have been downloaded and used for CLARA WebGIS. From the merging of the data contained therein, it has been possible to obtain a new shapefile consisting of 4043 buildings, each with information relating to building typology (Fig. 1A; masonry, reinforced concrete moment-resisting frame buildings, etc.), year of construction (Fig. 1B), use and state of conservation (Fig. 1C), and (eaves and maximum) heights (Fig. 1D). ISTAT shapefiles contain a series of census variables, the municipal administrative limits and the census sections of the study area, from which the SASSI area has been excluded (Fig. 1).

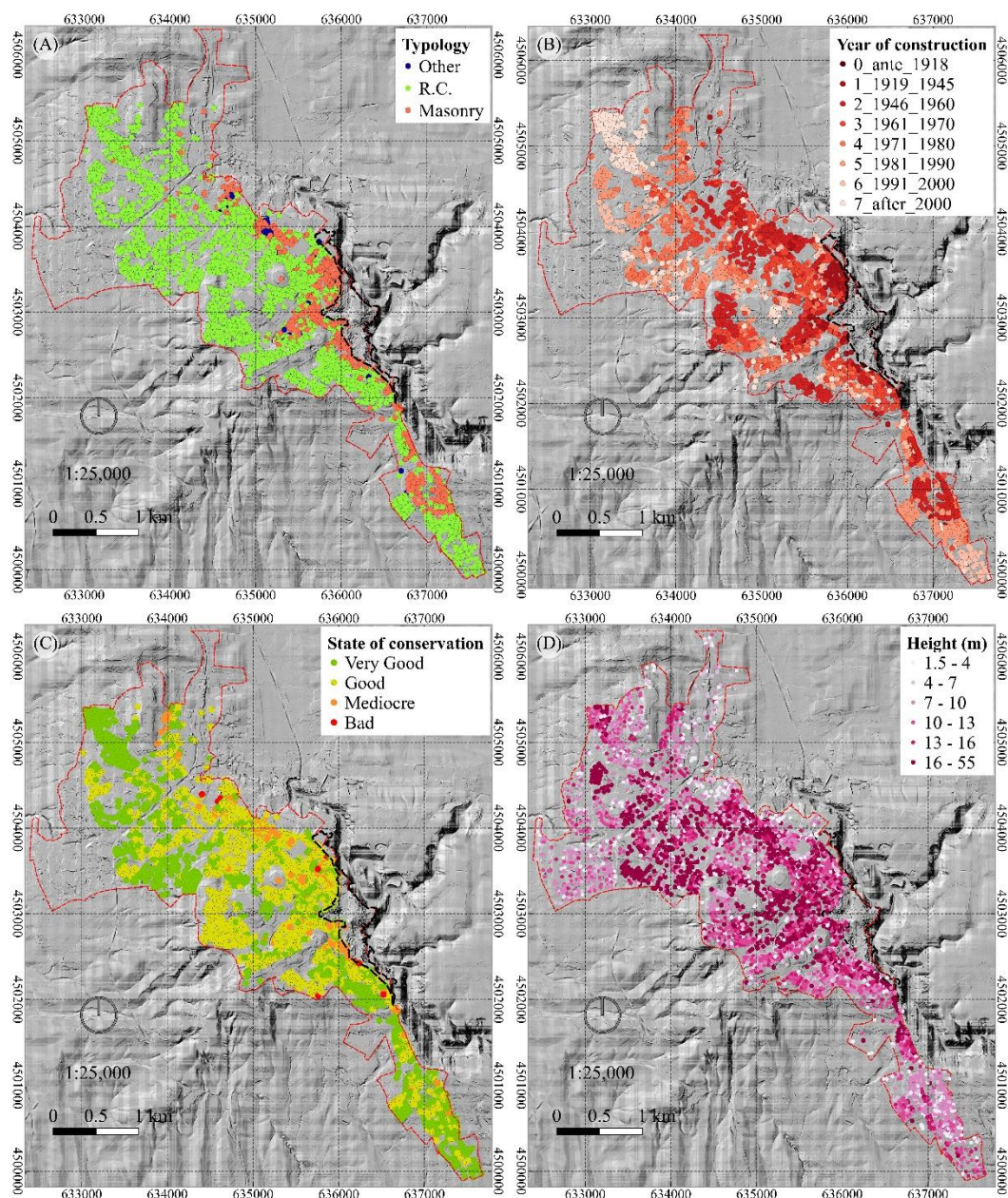


Figure 1. Spatial distribution of buildings characteristics: (A) building typology; (B) year of construction; (C) state of conservation; (D) height max (m). The black dashed line encloses the “SASSI” area (not included in this study). The red dashed line delimits the urban area on which the study is focused.

For 2648 buildings reported in OD Matera portal, there is a prevalence of reinforced concrete (~70%) compared to masonry (~27%) (Fig. 1A). In general, a good (~ 51%) and very good (~ 42%) state of conservation is reported for residential buildings, with few buildings in poor and mediocre conditions (~ 7%) which often correspond to those of older construction (as from last release, 14 February 2018) (Fig. 1B-C). The ISTAT data aggregated by neighbourhood allow us to make considerations and assessments on a territorial scale, i.e., the historic districts of the city (Piccianello, Historical Centre, Cappuccini-Agna) are mainly made up of masonry dwellings while the more recently urbanized districts show a prevalence of reinforced concrete moment-resisting frame buildings with a better state of conservation (Fig. 2).

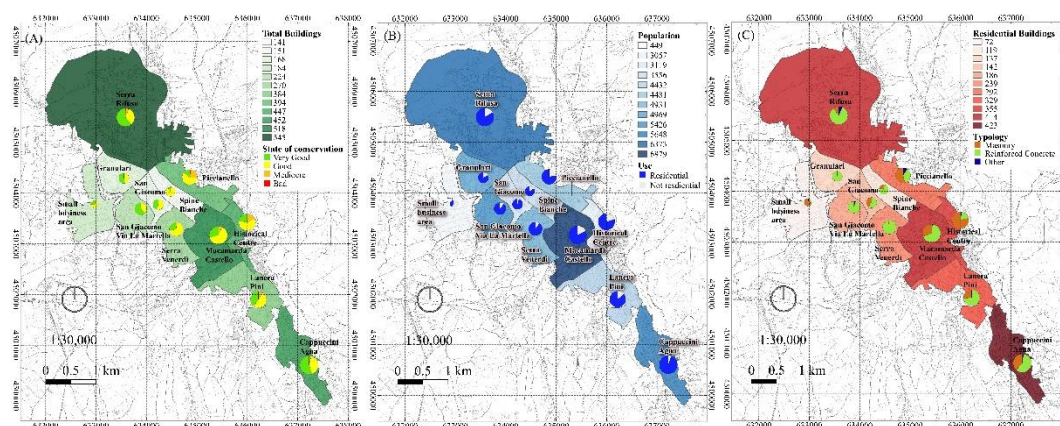


Figure 2. Spatial distribution of ISTAT census variables aggregated by neighbourhoods and classified according to (A) number of total buildings; (B) population; (C) number of residential buildings; with pie chart of: (A) buildings state of conservation; (B) use; (C) built typology.

2.2. Pre-existing Data

We have carried out a research, collection, digitization, and organization of the data available from previous studies carried out in the area of Matera. An archive made up of 319 georeferenced geological, geotechnical, geophysical, and seismic surveys (downholes, mechanical surveys, calcarenite sampling stations, MASW, HVNSR, seismic refraction surveys; Fig. 3) has been harmonized in a geo-database, ~11% of which consist of seismic surveys performed on buildings (Table 1). Moreover, the following maps of urban area derived from microzonation studies have been digitalized and georeferenced: geological, geomorphological and MOPS (homogeneous microzones from a seismic response perspective). The user can access, visualize, query, and download data via the WebGIS user interface by clicking on the geometries. The information display mode is possible at all levels, so after clicking on the geometry, the factsheets of all the active geometries arranged under the selected point will appear in nested mode (Fig. 3). Data can be downloaded by clicking on the hyperlink contained in the last row of each attribute table. We point out that ~87% of test certificates for geological-technical surveys are downloadable, and for the ~12.5% only the main results are available.

the text following an equation need not be a new paragraph. Please punctuate equations as regular text.

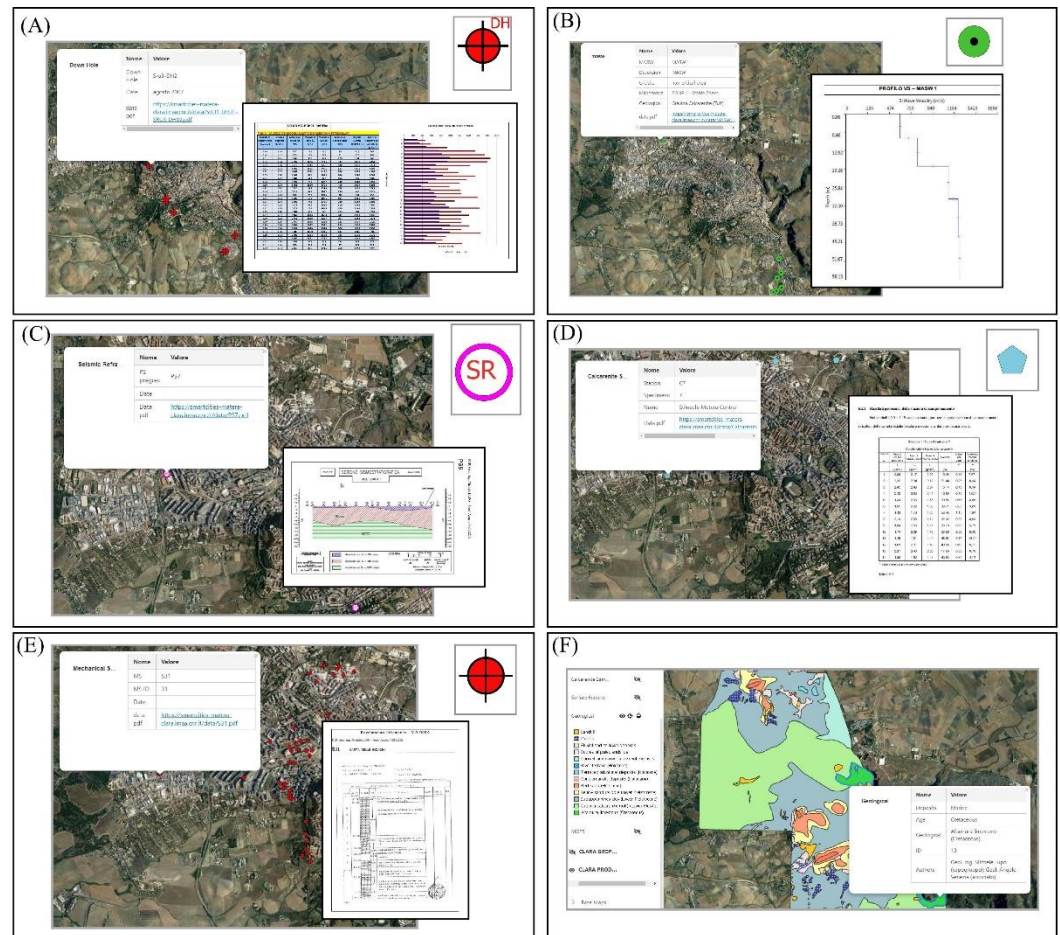


Figure 3. Example of factsheets displayed by clicking on the related geometries (polygon in F sub-image) or symbols (upper right corner of single sub-images A-E) and examples of downloadable file of pre-existing geological/geotechnical/geophysical surveys for: (A) Down-Hole; (B) seismic refraction survey; (C) mechanical survey; (D) MASW; (E) calcarenite sampling station; (F) geological map.

2.3. CLARA Data

2.3.1. Ground-based geophysical data

In the framework of the CLARA project, we have evaluated the interaction effect between near-surface geology and all overlying buildings in the urban area of the city of Matera as thoroughly described by [8]. To this end, we planned and performed 107 single-station seismic ambient noise measurements on the main urban lithologies and 62 on the main building typologies. All the seismic ambient noise recordings on soils and buildings were performed using Tromino seismographs (MoHo s.r.l.) and were analysed applying the Horizontal-to-Vertical spectral ratio technique (HVNSR) following the standard procedures [57-59] and using Grilla software (version 8.1, Moho s.r.l. 2018). We have been able to estimate the main resonance frequencies for all urban soils and the main vibrational frequencies for the measured buildings.

2.3.1.1. Soil HVNSR

The integration of the new 107 and 10 pre-existing HVNSR (Table 1) curves evaluated on urban soils has increased the area of the city of Matera covered by surveys from 18 to 1758 ha, with an average density of 3.7 surveys/Km². Overall, the density of all surveys in the urban area is about 11.25 surveys/Km². We merged in the same point-vector layer, named 'HVNSR soil', the pre-existing and new HVNSR functions. By clicking with the

hand icon cursor on the point of interest it is possible to visualize a factsheet with all the information related to that point (Fig. 4). The thirteen fields showed in the factsheet have been given self-explanatory names: 'X' and 'Y' report the coordinates or the measurement locations in UTM WGS84 33N, EPSG 32633; 'A_Threshold' is the value of the HVNSR amplitude beyond which amplification is considered to occur (this value has been chosen equal to 2 for all the analyses; Gallipoli et al., 2020 [8]); 'F0 soil' is the value of the soil fundamental resonance frequency (Hz) with an amplitude equal to 'A0 soil'; 'F1 soil' (< 'F0 soil') and 'F2 soil' (> 'F0 soil') are the two frequencies (Hz) at which the HVNSR curve intersects the 'A_Threshold' value; 'Data_asc' and 'Data_bmp' contains hyperlink to the downloadable HVNSR file in text format and HVNSR curve in .bmp format, respectively; vi) 'Macro area': indicates the neighbourhoods whose names are untranslatable except for 'Historical Center' ('Centro Storico') and 'Small business area' ('Zona Artigianale') [60].

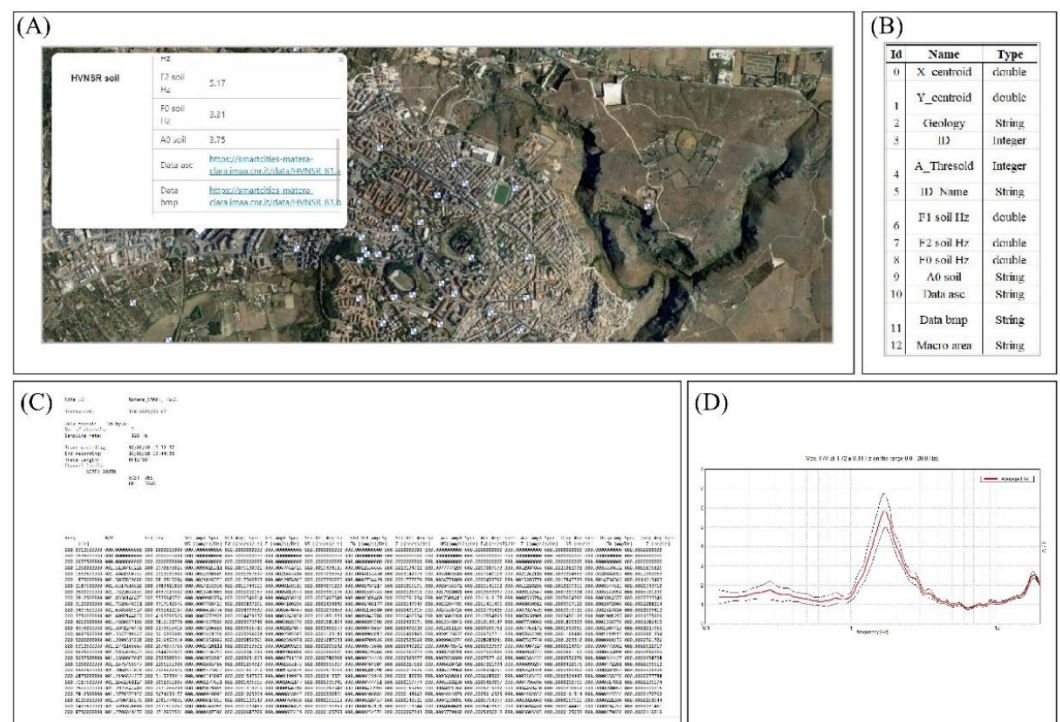


Figure 4. (A) Pop-up window showing the factsheet of an example measurement (HVNSR_51) made on soil; (B) type of the attributes; screenshots of downloadable (C) HVNSR text file and (D) HVNSR curve .bmp file.

2.3.1.2. Building HVNSR

By integrating the 34 pre-existing with the 62 new HVNSR functions estimated on buildings, the percentage of buildings measured has increased from 0.8% (#6) to 2.5% (#18) for masonry buildings (out of 732) and from 1.5% (#28) to 4.2% (#78) for reinforced concrete buildings (out of 1872). The percentage has been calculated respect to the total number of buildings falling within the studied area (#2648) for which the building typology is known. For reinforced concrete buildings, the sample distribution of measured buildings by macro-area is representative of the percentage of buildings in that area with respect to the total number of buildings in the urban study area (Fig. 5B-C). The same does not apply for masonry buildings (Fig. 5D-E) due to logistical issues (impossibility of access, etc.).

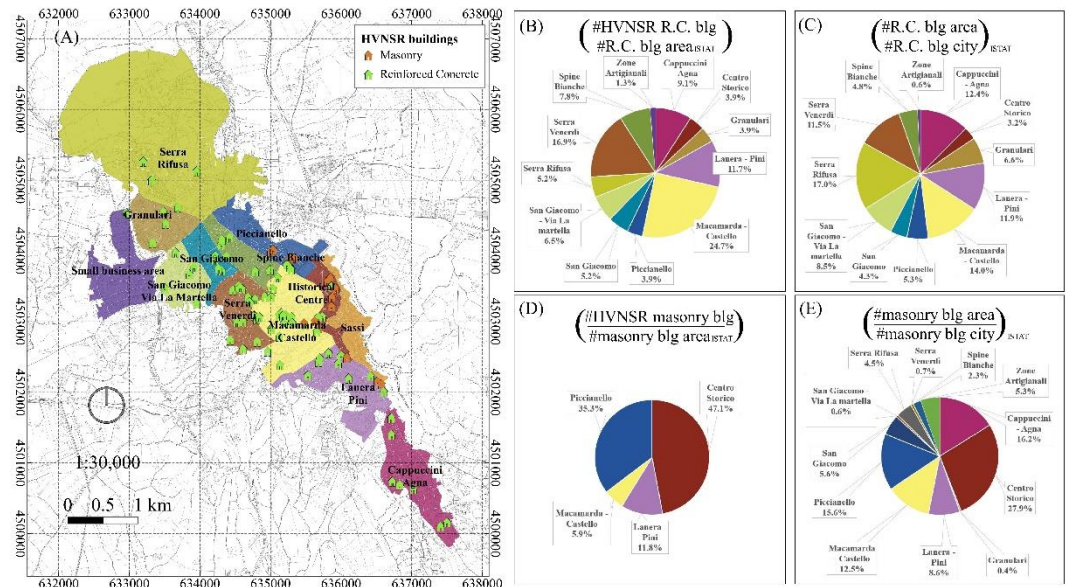


Figure 5. (A) Map of neighbourhoods and measured building locations along with pie charts showing proportion (as percentage) between measured and total number of buildings in the related macroarea for (B) reinforced concrete and (D) masonry; proportion (as percentage) of the number of buildings for each area with respect to the total number of buildings in the studied urban area for (C) reinforced concrete and (E) masonry according to census variables (ISTAT)

Except for the buildings in the “Granulari” districts or “Small business area”, which are almost completely founded on Gravina calcarenite, most of the buildings in the urban area of Matera lie on thick layers of Subappennines clays or above Gravina calcarenite (Fig. 6). A detailed presentation of the lithostratigraphic features of the area has been given by [8].

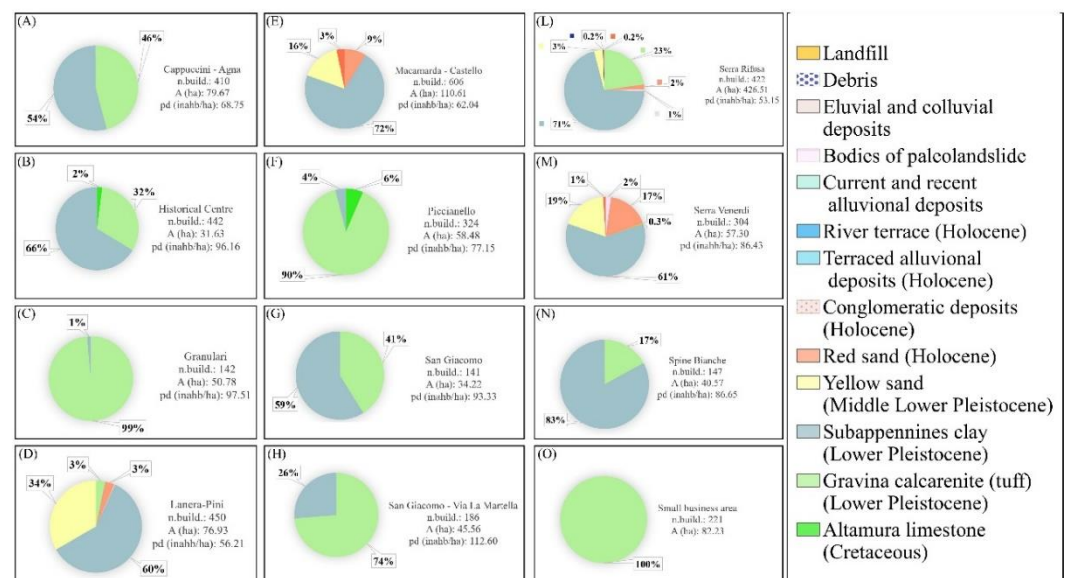


Figure 6. Pie charts showing proportion (as percentage) of major foundation soil geology for each macroarea. Every diagram reports the macro-area name, the number of buildings (n.build.), the extension of the area in hectares (A(ha)), and the population density expressed as inhab/ha (pd)

We merged all building HVNSRs in the same point-vector layer, named ‘HVNSR buildings’. The table attribute, available for consultation by clicking on a point, contains

fifteen fields with self-explaining names (Fig. 7): ‘X’ and ‘Y’ report the coordinates in UTM WGS84 33N, EPSG 32633; ‘Type’ refers to the building typology (R.C. or masonry); ‘F0 blg Hz’ is the main vibrational frequency of the building, retrieved by the HVNSR technique; ‘Use’ indicates the specific use for which a building is projected and built (i.e., residential, commercial, public, etc.); ‘Data asc zip’ and ‘Data bmp’ report the hyperlink of the downloadable HVNSR file in text format and HVNSR curve in .bmp format, respectively.

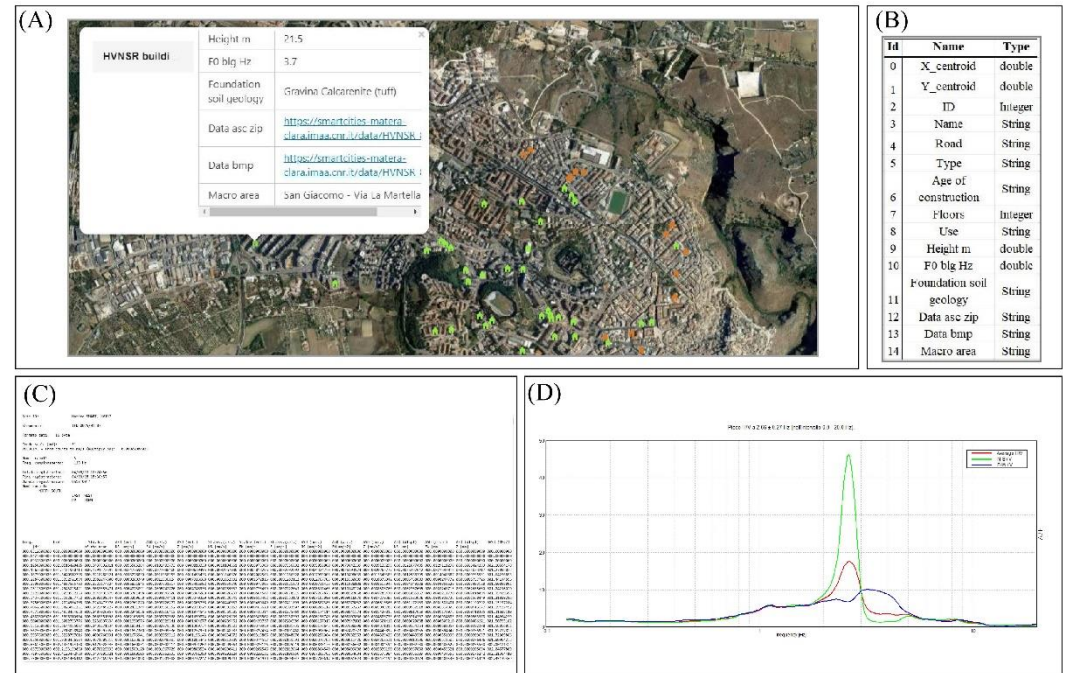


Figure 7. (A) Pop-up window showing the factsheet of an example measurement (HVNSR_69) made on a R.C. building; (B) attribute types; screenshots of downloadable (C) HVNSR text file and (D) HVNSR curve .bmp file.

2.3.2. Digital Surface Model from satellite data

DSMs represent the surface of the Earth as visible from space or air, which includes vegetation, buildings, infrastructures, and all human-made objects. They represent, therefore, an essential tool for a large variety of applications in engineering and science. In the framework of the CLARA project, we generated a DSM of the city of Matera and its surroundings, including the slope of the rocky ravine created by the Gravina stream [61]. In particular, we used the Agisoft Metashape photogrammetric software (Agisoft Metashape, 2021) [62] to process a cross-sensor multi-view satellite optical triplet composed of a WorldView-3 stereo pair and a GeoEye-1 image, whose acquisition features are described in [53].

We produced at first three DSMs using the three stereo pairs obtained by combining the three images. We followed the procedure described in [53] which adopts an original terrain-independent approach to refine the Rational Polynomial Coefficients (RPCs) supplied in each image metadata [63]. We applied the geoid undulations derived from the EGM2008 model [64] to transform the native ellipsoidal heights, derived from the RPC based orientation, to the corresponding orthometric ones. Moreover, we cropped the DSMs considering the maximum intersection area common to the three DSMs and we resampled our products to 0.5 m. Lastly, we produced the final DSM computing a weighted mean of the three DSMs [53].

Moreover, we computed an additional raster containing the building heights with respect to the ground level for each pixel belonging to a building, subtracting the heights of the RSDI Digital Terrain Model (DTM) - resampled to the DSM resolution - from the DSM heights.

To evaluate the accuracy of the overall DSM, we compared our product with a reference generated using the open data from RSDI. Specifically, we added the orthometric heights of the RSDI DTM, resampled to the DSM resolution, to the building eave heights of the shapefile called "unità volumetrica" to produce a reference DSM. In this way, we computed the height differences (ΔZ) between the reference and the overall DSM for each pixel (Fig. 8) and we evaluated the standard statistical indicators [65] (mean, standard deviation, root mean square error - RMSE, median, normalized median absolute deviation - NMAD, Linear Error at 68% and 90% confidence interval - LE68 and LE90). To compute the indicators, we adopted a threshold ΔZ equal to 20 m to remove the values outside the range ($-\Delta Z$, ΔZ) which were considered outliers.

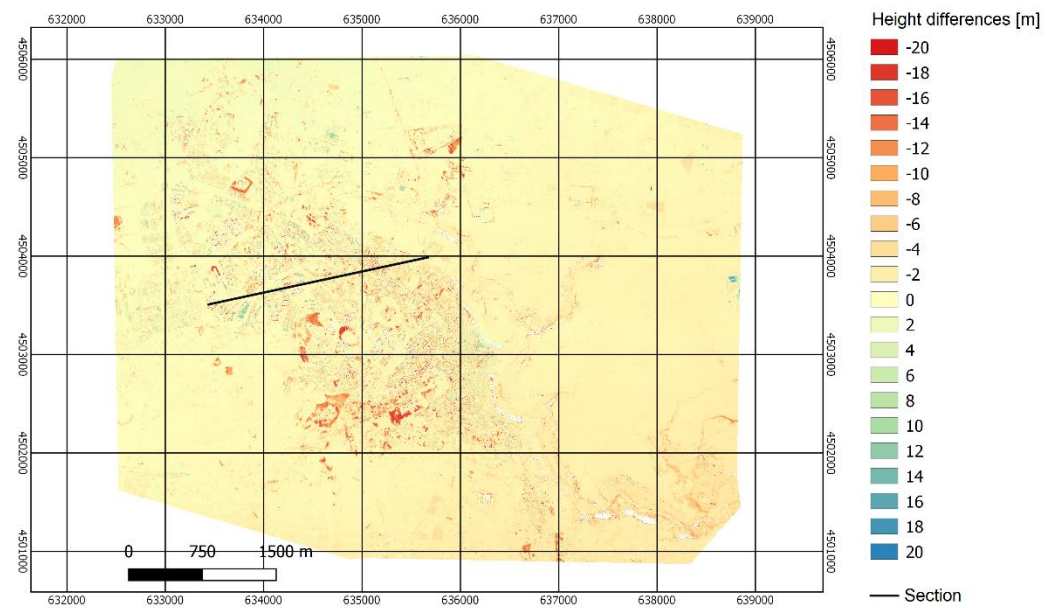


Figure 8. Error map (CRS: EPSG:32633-WGS 84/UTM, zone 33N-Projected) - height differences (in m) between the reference and the obtained DSM. The section of Fig. 10 is highlighted in black.

We assessed the results using the entire DSM and considering the different land covers separately. To distinguish artificial surfaces, agricultural, forest and semi-natural areas, we adopted the CORINE Land Cover inventory [66] at epoch 2012, resampled to the DSM resolution. Furthermore, we computed the statistics over the area corresponding exclusively to the buildings using the "unità volumetrica" shapefile. The results of the overall DSM validation are shown in Tab. 2. The DSM shows completeness equal to 98.42%, evaluated as the ratio (percentage) of the filled DSM pixels over the number of pixels of the reference raster.

Table 2. Statistical indicators for DSM accuracy assessment.

Tile	Mean [m]	Std. Dev. [m]	RMSE [m]	Median [m]	NMAD [m]	LE68 [m]	LE90 [m]	Number of pixels
Overall	-1.1	2.4	2.7	-0.8	1.1	1.2	3.0	119865099

Artificial surfaces	-1.3	3.7	3.9	-0.6	1.5	2.0	5.9	34110194
Agricultural areas	-0.8	1.6	1.8	-0.8	0.9	0.9	1.8	68037393
Semi-natural areas	-1.8	1.9	2.6	-1.4	1.0	1.2	2.7	17717512
Buildings	1.2	3.4	3.7	0.8	2.3	2.6	5.4	8110798

It is worth noticing that the errors in the semi-natural class can derive from the missing reconstruction of the vegetation in the reference DSM since it was generated from a DTM (Fig. 9). Moreover, the "Artificial Surfaces" and "Buildings" classes are the most critical due to the high urban density which makes, as known, the DSM production from satellite images very challenging because of occlusion issues (Fig. 10). For these two classes, the RMSE reaches the highest values, being slightly higher than 3.5 m. However, in this case, the values of median and NMAD, which are significantly lower than the mean and standard deviation, denote the presence of outliers. As mentioned, most of them are probably related to the occlusion issues; anyway, a careful inspection highlighted that some outliers can be due to rather coarse simplifications inside the "unità volumetrica" shapefile which was used to generate the reference for the buildings. In fact, some complex buildings (one relevant example is the Castle - Fig. 9) were represented with just a unique height. Therefore, it has to be considered the possibility to improve the building heights in RSDI using the generated DSM where outliers were highlighted.

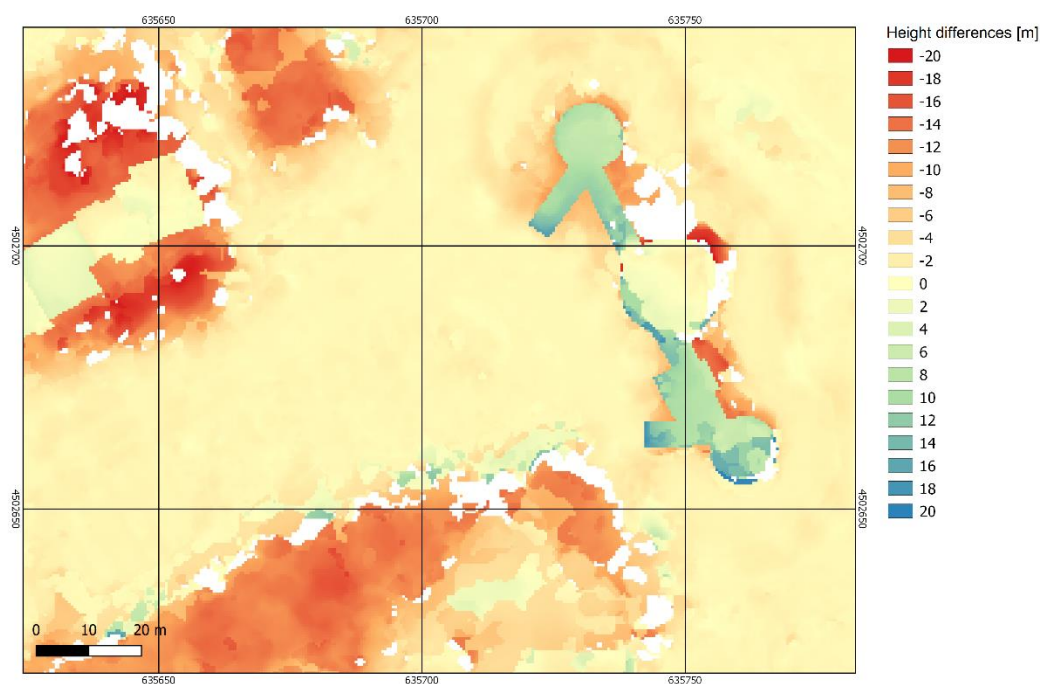


Figure 9. Error map (CRS: EPSG:32633-WGS 84/UTM, zone 33N-Projected) - height differences (in m) between the reference and the obtained DSM: detail of the castle area, where the highest errors are due to the missing vegetation in the DTM and to the coarse unique height in the reference, derived from the "unità volumetrica" shapefile (the two wings of the castle are shorter than the central tower, but they are registered with the same height in the shapefile).

Finally, Fig. 10 shows a section extracted from the reference (in black) and the generated DSM (in red); as indicated in the lower left and lower right corners, the profile direction is SW-NE (Fig. 8). Even if the resulting DSM is noisier than the reference, the multi-view approach allows to accurately and densely reconstruct the terrain and all the objects insisting on it (buildings - visible in the reference - and vegetation - not included).

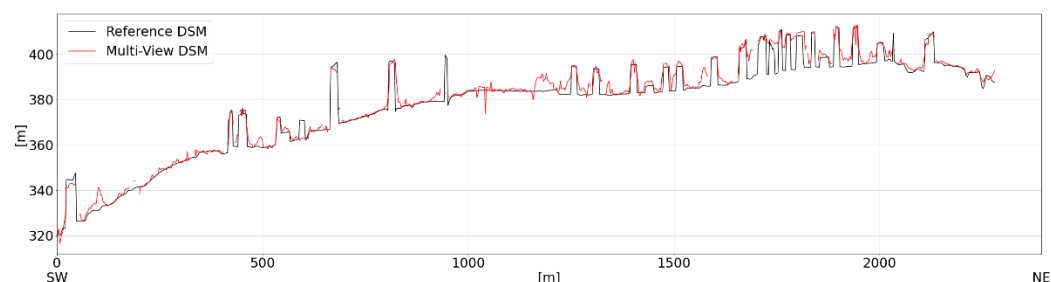


Figure 10. Section extracted from the reference DSM and the DSM generated with the multi-view approach.

3. CLARA WebGIS products

3.1 Soil isofrequency, soil iso-amplitude and building frequency distribution maps

Interpolating the soil resonance frequency values ('F0 soil Hz') and the relative amplitude values ('A0 soil'), which derive from the HVSR analysis on the measurements carried out at each of the urban soil 117 locations, we retrieved the soil isofrequency (Fig. 11-A) and isoamplitude maps (Fig. 11-B), respectively. By clicking on any cell of the 'Soil isofrequency' (or 'Soil isoamplitude') map layer a factsheet in multi-level form shows the interpolated 'F0 soil Hz' (or amplitude 'A0 soil') value. Using the empirical relationship $T = 0.0167 H$ estimated for the measured buildings [8] and having available the heights for all buildings of the Matera City, we have predicted the main vibrational frequency and its uncertainty ('F0 blg range Hz') for 4043 buildings. By clicking on any geometry of the 'Building frequency' layer, the user can visualize both the estimated main vibrational frequency of the building 'F0 blg Hz' and the interpolated frequency of its foundation soil 'F0 soil Hz' values in the same factsheet (Fig. 11-C).

The building's first vibrational frequencies ('F0 blg Hz) and the soil's fundamental frequencies ('F0 soil Hz') are classified based on the same frequency ranges and colour palette, so that a building and the underlying soil pixel having the same colour means that they vibrate in the same range of frequencies (Fig. 11-C). This layer has an attribute table composed by thirteen fields (Fig. 11-C.2), most of them inherited from the layers presented above. New fields are: 'Class f b' indicates the class of frequency range ('Fo b range Hz') to which the building belongs, reported in the penultimate row of the factsheet.

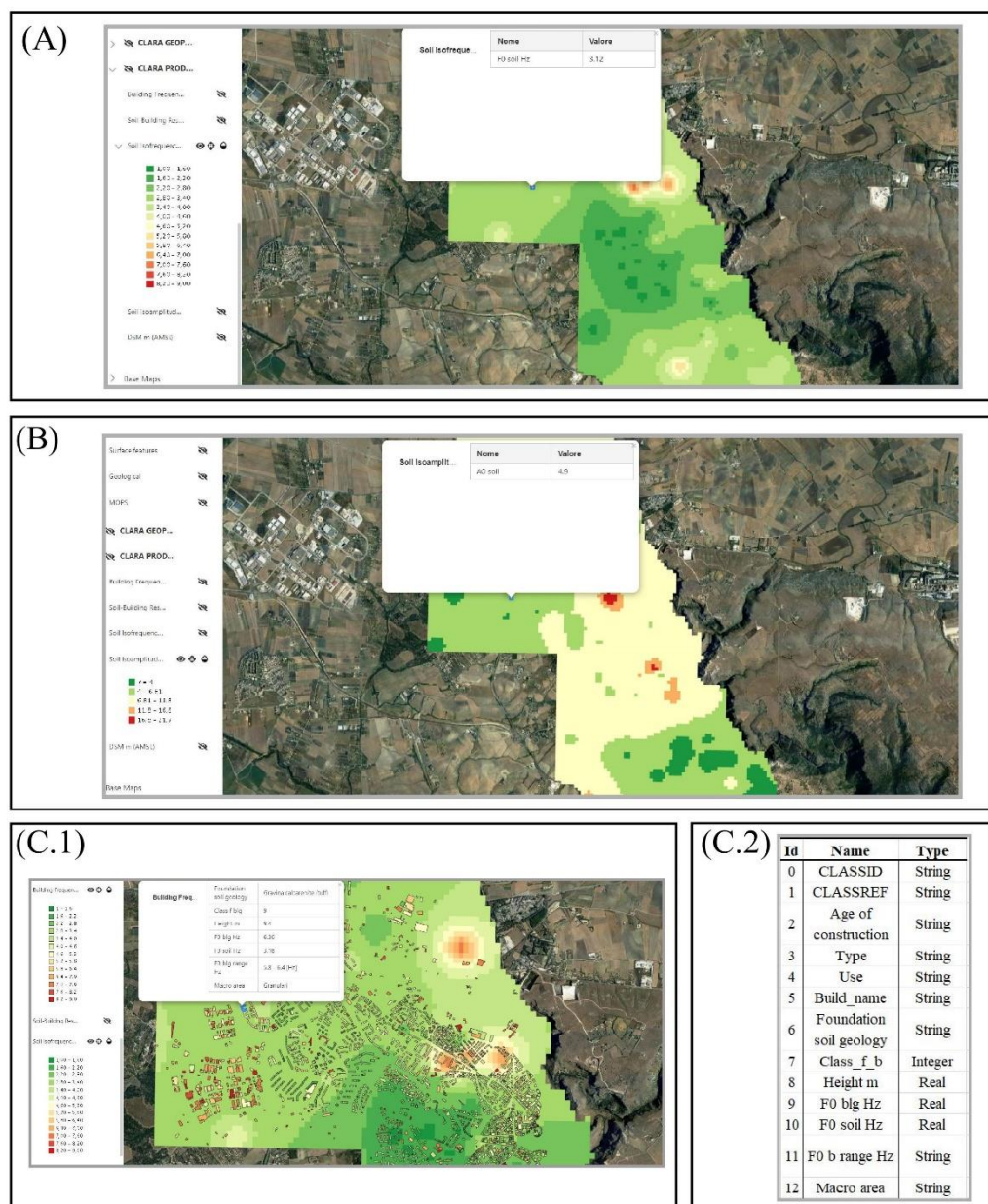


Figure 11. Screenshot of mapview and pop up showing: (A) soil isofrequency map; (B) soil isoamplitude map; (C.1) building frequency distribution overlaying soil isofrequency map. The building frequency layer has an attribute table composed of thirteen fields (C.2).

3.2 Soil – building resonance map

The soil-building resonance effect was evaluated considering the overlap between the amplifying HVNSR frequency ranges of the soil ('F1 soil Hz' - 'F2 soil Hz') and buildings ('F1 blg Hz' and 'F2 blg Hz') as shown in [8]. We have identified six levels of probability of soil-building resonance occurrence encoded through a color scale ranging from green (low probability of resonance occurrence) to red (high probability of resonance occurrence). A building whose estimated range of resonance falls within the interpolated resonance range of the underlying soil is attributed a high probability of resonance occurrence (100%, colored red), whereas a low probability level is assigned when the estimated resonance range of the building is completely disjoint from that of the interpolated underlying soil (Fig. 12). By clicking on any of the 4043 polygons in the 'Soil-building resonance levels' an attribute table containing fourteen fields pops up. Most of the entries of the factsheet are inherited from other layers except a new one named 'resonance level' that reports the concatenation of three information: the class (of resonance occurrence

probability) to which the building belongs to, the total number of buildings in that same class, and the percentage with respect to the analysed building stock (4043).

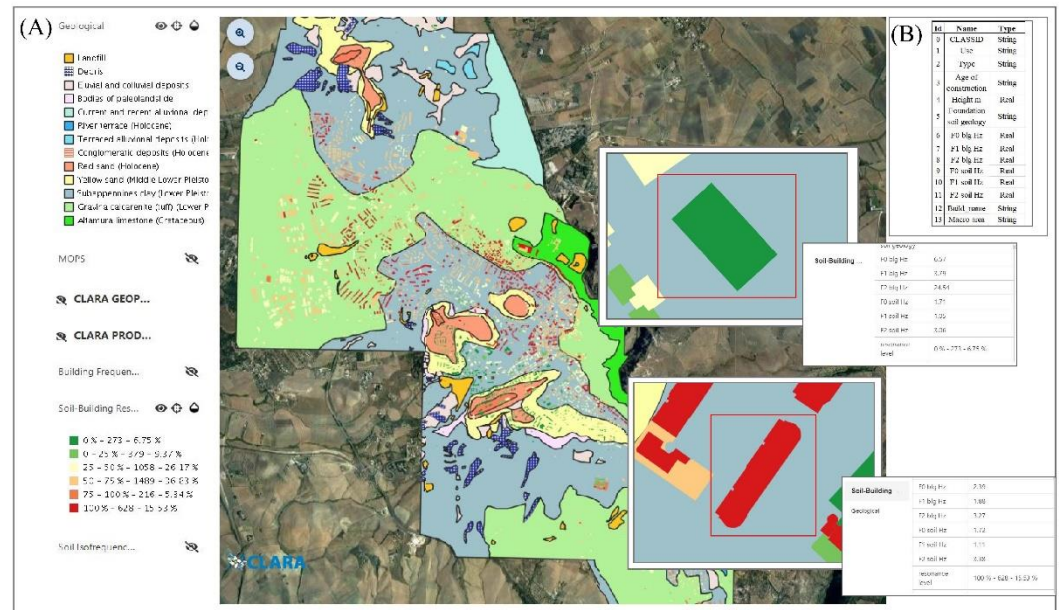


Figure 12. (A) Screenshot of soil – building resonance levels overlapped to the geological map in the urban area of Matera. The insets show two examples: a (red-colored) building having ‘F1 blg Hz’ and ‘F2 blg Hz’ values included in the interpolated soil frequency range (100% probability of resonance occurrence), and a (green-colored) building with a probability of resonance effect equal to 0 %, along with the related pop-up windows; (B) attribute table of soil building resonance level layer.

3.3 Digital Surface Model and Building height rasters

The DSM raster has a resolution of 0.5x0.5 m and covers an area ranging from 632450.2 m E to 638868.7 m E and from 4500872.2 m N to 4506039.2 m N (Coordinate Reference System CRS: EPSG:32633-WGS 84/UTM, zone 33N-Projected). The elevations, expressed in meters, are orthometric heights referred to EGM2008 geoid model. Among the 121'879'530 pixels of the raster, 1'921'658 (1,58%) have no height information: these void pixels are indeed located within the urban area, near and among the buildings, and in the deepest valleys of the rocky ravine, where the occlusions and shadows have a negative impact on the photogrammetric matching process. By clicking on any point of the layer, it is possible to visualize the height value of each pixel inside the raster (Fig. 13).

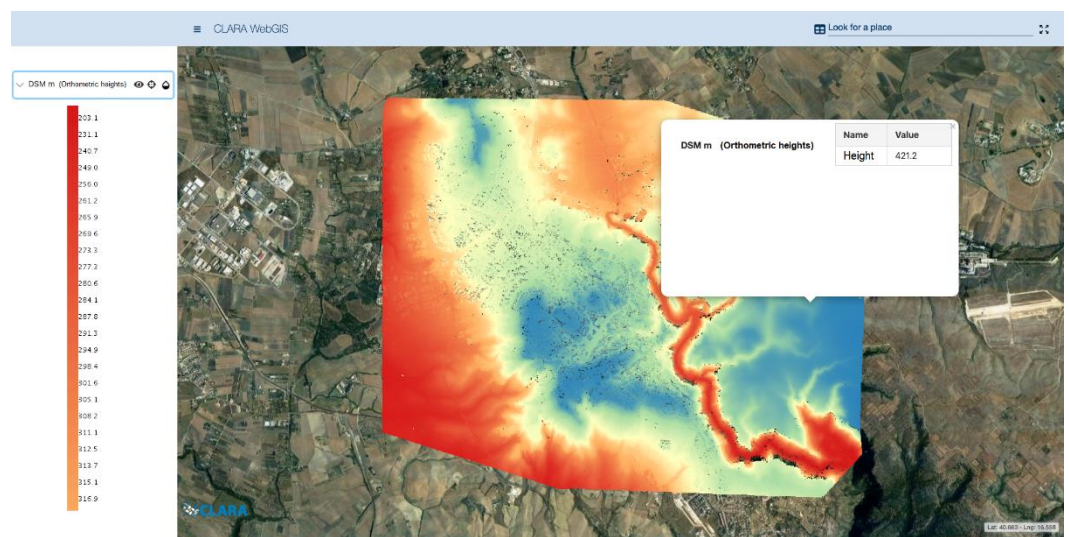


Figure 13. DSM raster (CRS: EPSG:32633-WGS 84/UTM, zone 33N-Projected).

The building height layer is a masked raster in which only the pixels corresponding to the buildings contain the height (expressed in meters) of the considered building with respect to the ground (Fig. 14). It is important to highlight that this height is different from the eave height - which is the facade height (Fig. 14). The building height raster covers the same area of the DSM raster and is characterized by the same resolution (0.5 m) and CRS.

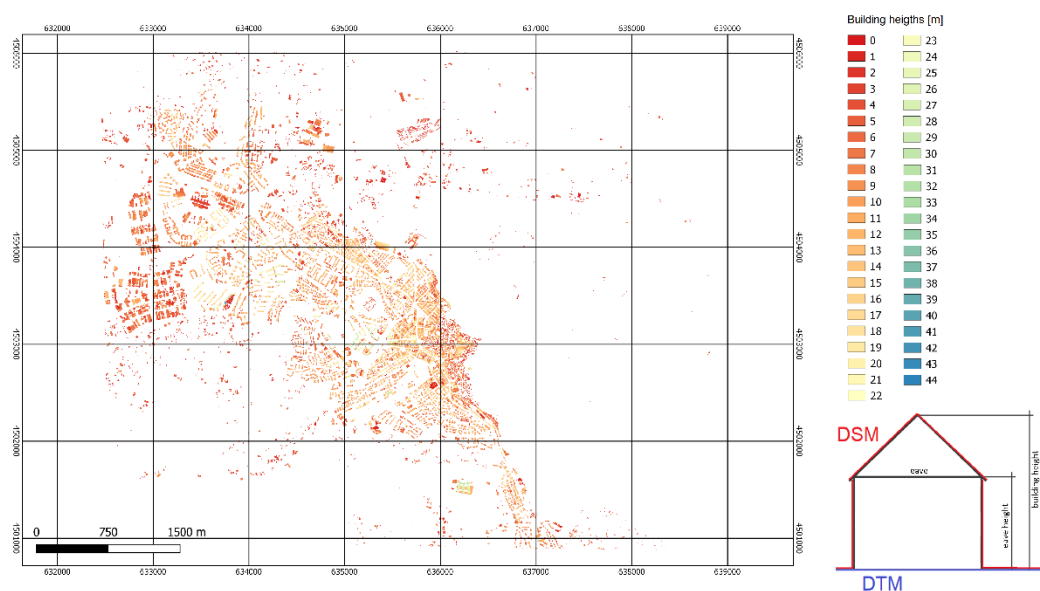


Figure 14. Building height raster (CRS: EPSG:32633-WGS 84/UTM, zone 33N-Projected). The building height is obtained as the difference between the DSM and the DTM and it should not be confused with the eave height, i.e., the facade height.

4. Discussions

If societies do not preserve the memory of historical earthquakes and do not build up the culture of seismic risk, earthquakes will continue to have catastrophic effects [67, 68]. The improvement of the knowledge and awareness of individual citizens is key for achieving a better resilience of civil communities. In this view, sharing information about the seismic aspects peculiar to a given urban environment with the widest target of end users possible (administrators and planners central and local, engineers and professional geologists, citizens, etc.) constitutes a correct behavior, which is nowadays supported by the emerging paradigm of open data and the modern geospatial technologies. Aiming at improving seismic risk mitigation of the city of Matera, CLARA WebGIS has indeed been designed to organise, analyze, and disseminate the available information on soil, buildings and on soil–building interaction in the urban area of Matera combining open data availability with new geospatial technologies. In the following, we try to highlight some useful aspects that we have identified in relation to those we believe to be the main users, or beneficiaries of this tool, i.e., local authorities, urban planners, freelancers, and private citizens.

4.1 CLARA WebGIS potential and perspectives

The knowledge of the spatial distribution of the local seismic amplification effect, of the main characteristics of buildings, and of the soil – building resonance effect contribute to reach more efficiently a threefold objective: i) increase the seismic resilience of urban system reducing the probability that a crisis occurs in case of earthquake; ii) reduce the potential losses in economic and social terms; iii) facilitating the return of the urban system to pre-existing conditions or recovering a new state of equilibrium by reducing the recovery phases time.

If we share the basic principle according to which the use of the areas affected by seismic amplification and their secondary effects (road obstruction, interruption of services, slowdown of rescue services, etc.) should be more carefully regulated, then the mapping of the probability of occurrence of soil-building resonance along with the consequent assessment of the areas with the greatest probability of increased damage during seismic events become crucial for the implementation of mitigation and prevention strategies (urban planning laws, land use planning, plans of intervention for emergencies and to manage post-earthquake crisis). For example, the soil-structure interaction maps in the urban area of cities could help: i) to discriminate the most suitable areas for urbanization (characterized by low resonance level) or eligible for other intended use such as parks, gardens, recreational areas (characterized by medium / low resonance); ii) to define seismic retrofitting strategies for existing strategic buildings/structures/infrastructures; iii) to integrate microzonation studies with the effects due to the presence of buildings and their interaction with the soil according to a holistic approach [8]. The achievement of the latter two targets is all the more feasible since some governments are currently financing seismic retrofitting for existing buildings and microzonation studies, e.g. the Italian government through “Sisma bonus” (Ministerial Decree August 6, 2020, n. 329) [69] and ‘Guidelines for Seismic Microzonation’ [70] respectively.

For years, technical and scientific communities have been discussing the opportunity of creating for each building a certificate containing all the information available. Besides basic information on each building (height, age of construction, typology, use, etc...) and, geological/geotechnical data of the relative foundation soil, the CLARA WebGIS contains the estimates of the fundamental frequency of all urban soils and the vibrational frequency in the linear elastic domain for 4043 buildings within the urban area. Such information constitutes invaluable knowledge for freelance engineers as it is key for numerical models of seismic retrofitting.

In addition, CLARA WebGIS allows making further evaluations to support mitigation strategies, both on an urban and suburban scale by crossing the geophysical and engineering data contained in the layers. For example, by cross-referencing the data on the state of conservation of buildings with the probability levels of soil-building resonance occurrence, it is possible to estimate the number of buildings for which seismic retrofitting is recommended (Fig. 15).

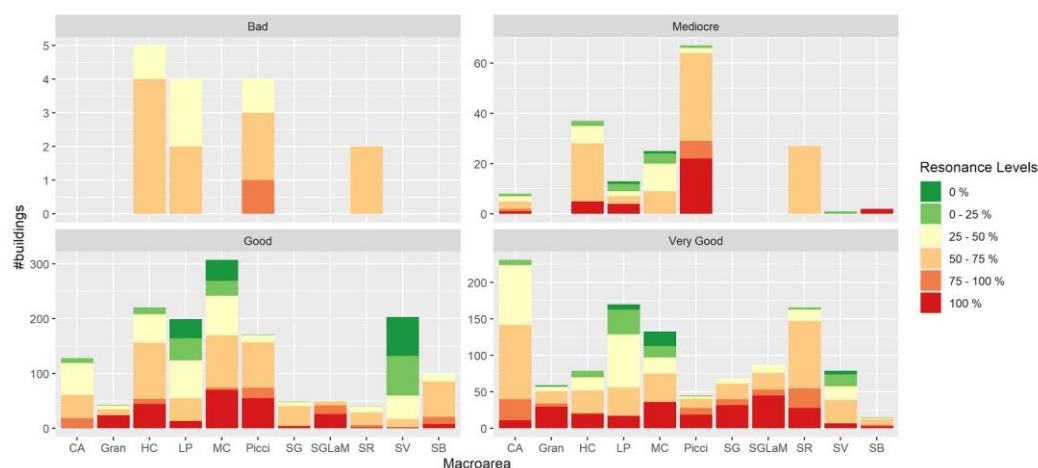


Figure 15. Bar charts showing the number of buildings for each macroarea highlighting the probability levels of resonance occurrence and the building state-of-conservation. CA: Cappuccini - Agna; Gran: Granulari; HC: Historical Centre; LP: Lanera - Pini; MC: Macamarda - Castello; Picci: Piccianello; SG: San Giacomo; SGLaM: San Giacomo - Via La Martella; SV: Serra Venerdi; SV: Serra Rifusa.

The experience gained in the development of the CLARA WebGIS, with respect to the creation of a digital surface model (DSM) starting from the elaboration of satellite data,

can constitute an adaptable reference for those situations in which there is no availability of open data on building heights. Indeed, if DSMs, which represent the Earth surface with all the human-made objects insisting on it (including precise information on the orthometric heights of buildings and infrastructures), are accompanied by the orthometric elevation of the topographic surface (provided by a digital terrain or elevation model – a DTM or a DEM), allow retrieving an accurate estimate of the height from ground for each building. Moreover, for DSMs generated from high-resolution satellite imagery, the RMSE of the height estimate can reach a few meters (up to 3.5 m, as is the case of this study, which corresponds to an overestimate or underestimate of one floor for each building). Thanks to this estimate (whose level of accuracy may be possibly increased in the coming years with the development of new sensors) and to a detailed information on the type of foundation soil, it would still be possible to evaluate the resonance frequency of the buildings (inversely proportional to their heights) in areas where data on building heights are totally absent (or not publicly available), and thus to predict the type of response of each building to a seismic event.

In our vision, in the time to come the following goals need to be pursued: 1) the CLARA WebGIS should be continuously developed and updated taking into account additional needs, future challenges, user feedback and the best available ICT; 2) the management of CLARA WebGIS should be entrusted to local administrators to ensure greater efficiency in its updating, maintenance, and above all to strengthen awareness of the perception of risk in the actors responsible for implementing mitigation strategies.

5. Conclusions

In this paper, we have presented the interactive CLARA WebGIS (<https://smartcities-matera-clara.imaa.cnr.it/>), a useful tool to visualize geological, geotechnical and geophysical data for urban soils, the main characteristics of the overlying buildings and a new DSM of the city of Matera. The CLARA WebGIS geodatabase, developed, maintained and enriched by CNR – IMAA, and managed by CNR – GeoSDI, has been released in the framework of CLARA project (CLOUD pLATFORM and smart underground imaging for natural Risk Assessment). The WebGIS has been built using open-source software and with a user-friendly interface as it is addressed to a wider target of end users (government administrators and planners, engineers and geologists, citizens, etc.). The database contains 319 geological and geotechnical surveys (Downholes, Mechanical Surveys, Calcarenite Sampling Stations, MASW, HVNSR, Seismic Refraction Surveys) performed in previous studies during 1990-2010, a geological and geomorphological map, a map of homogeneous microzones in a seismic perspective and 213 new single-station seismic ambient noise measurements carried out between 2015 and 2019 during CLARA project. The principal outputs derived by crossing all geophysical and engineering data available in the database are: 1) the estimation of fundamental resonance frequency for all urban soils; 2) the estimation of the main vibrational frequencies for 4043 overlying buildings; 3) the resonance effect of each building with respect to the relative foundation soil; 4) the DSM generated using a triplet of satellite imagery composed of a WorldView-3 stereo pair and a GeoEye-1 image, and a building height map obtained from the produced DSM and the RSDI open data. The first three outputs, regarding the main soil and building characteristics and their interaction, represent a key element to plan strategies for seismic risk mitigation in terms of urban planning, seismic retrofitting, and management of post-earthquake crises. Moreover, the detailed DSM could represent an improving knowledge for those cities/megacities without open data on building heights. We hope that this tool can be a starting point for administrations of all cities, that is, that they can build a geodatabase similar to CLARA webGIS by putting together pre-existing and new geophysical data for the characterization of the soil and buildings.

Author Contributions: Conceptualization, M.R.G.; methodology G.C., L.L., V.B., R.R. and M.R.G.; software, N.T., G.C., L.L., V.B., R.R. and V.S.; validation, L.L., V.B., R.R. and M.R.G.; formal analysis,

N.T., G.C., L.L., V.B. and R.R.; investigation, N.T., G.C. and M.L.; resources, N.T., G.C., M.L., V.S. and M.R.G.; data curation, N.T., G.C., L.L., V.B. and R.R.; writing - original draft preparation, N.T., G.C., L.L., V.B., R.R. and M.R.G.; writing – review and editing, G.C. and M.R.G.; visualization N.T., G.C., L.L., V.B. and R.R.; supervision, M.R.G.; project administration, M.R.G.; funding acquisition, M.R.G. All authors have read and agreed to the published version of the manuscript.

Funding: This research was funded by project CLARA (Cloud pLATFORM and smart underground imaging for natural Risk Assessment, id code n. SCN_00451, funded by the Italian Ministry of University and Research).

Data Availability Statement: The data presented in this study are openly available in <https://smartcities-matera-clara.imaacnr.it/>

Acknowledgments: We like to thank our research colleagues Angela Perrone (CNR IMAA, Tito Scalo - Potenza) and Prof. Mattia Crespi (Geodesy and Geomatics Division, DICEA, Sapienza University of Rome, Rome, Italy) for their helpful suggestions to improve the manuscript. The authors gratefully acknowledge the geoSDI team, who edited the online publication of WebGIS, particularly to Dr. Donato Maio and Eng. Lorenzo Amato for their valuable support, cooperation, and precious assistance to the activities of the platform. A final word of gratitude is expressed to the owners of the buildings who kindly provided their valuable time to let us do ambient noise measurements.

Conflicts of Interest: The authors declare no conflict of interest.

References

- 2014 revision of the World Urbanization Prospects. **2014**.
- Steffen, W.; Sanderson, A.; Tyson, P.; Jäger, J.; Matson, P.; Moore, B.; Oldfield, F.; Richardson, K.; Schellnhuber, H.J.; Turner, B.L.; et al. *Global Change and the Earth System; Global Change — The IGBP Series; Springer Berlin Heidelberg: Berlin, Heidelberg, 2005; ISBN 978-3-540-26594-8*.
- Nations Office for Disaster Risk Reduction, U. Sendai Framework for Disaster Risk Reduction 2015 - 2030;
- Transforming our world: the 2030 Agenda for Sustainable Development | Department of Economic and Social Affairs Available online: <https://sdgs.un.org/2030agenda> (accessed on Mar 30, 2021).
- The Urban Agenda for the EU - Regional Policy - European Commission Available online: https://ec.europa.eu/regional_policy/en/policy/themes/urban-development/agenda/ (accessed on Mar 31, 2021).
- Lapenna, V. Resilient and sustainable cities of tomorrow: the role of applied geophysics. **2017**, *58*, 237–251, doi:10.4430/bgta0204.
- Bellanova, J.; Calamita, G.; Catapano, I.; Ciucci, A.; Cornacchia, C.; Gennarelli, G.; Giocoli, A.; Fisangher, F.; Ludeno, G.; Morelli, G.; et al. GPR and ERT Investigations in Urban Areas: the Case-Study of Matera (Southern Italy). *Remote Sens.* **2020**, *12*, 1879, doi:10.3390/rs12111879.
- Gallipoli, M.R.; Calamita, G.; Tragni, N.; Pisapia, D.; Lupo, M.; Mucciarelli, M.; Stabile, T.A.; Perrone, A.; Amato, L.; Izzì, F.; et al. Evaluation of soil-building resonance effect in the urban area of the city of Matera (Italy). *Eng. Geol.* **2020**, *272*, doi:10.1016/j.enggeo.2020.105645.
- Lapenna*, V. CLoud pLATFORM and smart underground imaging for natural risk assessment in urban areas: The Clara project. In *Proceedings of the Global Meeting Abstracts; Society of Exploration Geophysicists, 2019; pp. 18–18*.
- Massolino, G.; Sandron, D.; Gallipoli, M.R.; Rebez, A.; Mucciarelli, M.; Stabile, T.A. Ambient vibration measures on strategic buildings in Matera in the framework of the CLARA-Smart Cities project; 2016;
- Shi, X.; Yang, G.; Yu, D.; Xu, S.; Warner, E.D.; Petersen, G.W.; Sun, W.; Zhao, Y.; Easterling, W.E.; Wang, H. A WebGIS system for relating genetic soil classification of China to soil taxonomy. *Comput. Geosci.* **2010**, *36*, 768–775, doi:10.1016/j.cageo.2009.10.005.
- Manna, P.; Bonfante, A.; Colandrea, M.; Di Vaio, C.; Langella, G.; Marotta, L.; Mileti, F.A.; Minieri, L.; Terribile, F.; Vingiani, S.; et al. A geospatial decision support system to assist olive growing at the landscape scale. *Comput. Electron. Agric.* **2020**, *168*, 105143, doi:10.1016/j.compag.2019.105143.
- (PDF) WebGIS e divulgazione del dato archeologico con software open source. Il progetto “Siponto aperta” | Ginevra Panzarino - [Academia.edu](https://www.academia.edu) Available online: https://www.academia.edu/20286522/WebGIS_e_divulgazione_del_dato_archeologico_con_software_open_source_Il_progetto_o_Siponto_aperta_ (accessed on Mar 31, 2021).
- Colucci, E.; Spanò, A.; Chiabrandò, F. WebGIS tools to disseminate archaeological landscape memory. **2017**, *2*, 3, doi:10.14609/Ti_2_17_3e.
- Filocamo, F.; Di Paola, G.; Mastrobuono, L.; Roskopf, C.M. MoGeo, a Mobile Application to Promote Geotourism in Molise Region (Southern Italy). *Resources* **2020**, *9*, 31, doi:10.3390/resources9030031.
- Müller, M.; Vorogushyn, S.; Maier, P.; Thicken, A.H.; Petrow, T.; Kron, A.; Büchele, B.; Wächter, J. CEDIM Risk Explorer - A map server solution in the project “Risk Map Germany.” *Nat. Hazards Earth Syst. Sci.* **2006**, *6*, 711–720, doi:10.5194/nhess-6-711-2006.

17. Frigerio, S.; Van Westen, C.J. RiskCity and WebRiskCity: Data collection, display, and dissemination in a multi-risk training package. *Cartogr. Geogr. Inf. Sci.* **2010**, *37*, 119–135, doi:10.1559/152304010791232190.
18. Frigerio, S.; Kappes, M.; Blahút, J.; Skupinski, G. The use of geo-information and modern visualization tools for risk communication. In *Advances in Natural and Technological Hazards Research*; Springer Netherlands, 2014; Vol. 34, pp. 383–407.
19. Fago, P.; Pignatelli, C.; Piscitelli, A.; Milella, M.; Venerito, M.; Sansò, P.; Mastronuzzi, G. WebGIS for Italian tsunamis: A useful tool for coastal planners. *Mar. Geol.* **2014**, *355*, 369–376, doi:10.1016/j.margeo.2014.06.012.
20. Aye, Z.C.; Sprague, T.; Cortes, V.J.; Prenger-Berninghoff, K.; Jaboyedoff, M.; Derron, M.H. A collaborative (web-GIS) framework based on empirical data collected from three case studies in Europe for risk management of hydro-meteorological hazards. *Int. J. Disaster Risk Reduct.* **2016**, *15*, 10–23, doi:10.1016/j.ijdrr.2015.12.001.
21. Aye, Z.C.; Jaboyedoff, M.; Derron, M.H.; Van Westen, C.J.; Hussin, H.Y.; Ciurean, R.L.; Frigerio, S.; Pasuto, A. An interactive web-GIS tool for risk analysis: A case study in the Fella River basin, Italy. *Nat. Hazards Earth Syst. Sci.* **2016**, *16*, 85–101, doi:10.5194/nhess-16-85-2016.
22. Huang, J.; Huang, R.; Ju, N.; Xu, Q.; He, C. 3D WebGIS-based platform for debris flow early warning: A case study. *Eng. Geol.* **2015**, *197*, 57–66, doi:10.1016/j.enggeo.2015.08.013.
23. Thiebes, B.; Bell, R.; Glade, T.; Jäger, S.; Anderson, M.; Holcombe, L. A WebGIS decision-support system for slope stability based on limit-equilibrium modelling. *Eng. Geol.* **2013**, *158*, 109–118, doi:10.1016/j.enggeo.2013.03.004.
24. Oppikofer, T.; Nordahl, B.; Bunkholt, H.; Nicolaisen, M.; Jarna, A.; Iversen, S.; Hermanns, R.L.; Böhme, M.; Yugsi Molina, F.X. Database and online map service on unstable rock slopes in Norway - From data perpetuation to public information. *Geomorphology* **2015**, *249*, 69–81, doi:10.1016/j.geomorph.2015.08.005.
25. Salvati, P.; Balducci, V.; Bianchi, C.; Guzzetti, F.; Tonelli, G. A WebGIS for the dissemination of information on historical landslides and floods in Umbria, Italy. *Geoinformatica* **2009**, *13*, 305–322, doi:10.1007/s10707-008-0072-1.
26. Pessina, V.; Meroni, F. A WebGis tool for seismic hazard scenarios and risk analysis. *Soil Dyn. Earthq. Eng.* **2009**, *29*, 1274–1281, doi:10.1016/j.soildyn.2009.03.001.
27. Bozzoni, F. Seismic risk assessment of seaports using GIS: the port of Gioia Tauro in Southern Italy.
28. Francini, M.; Artese, S.; Gaudio, S.; Palermo, A.; Viapiana, M.F. To support urban emergency planning: A GIS instrument for the choice of optimal routes based on seismic hazards. *Int. J. Disaster Risk Reduct.* **2018**, *31*, 121–134, doi:10.1016/j.ijdrr.2018.04.020.
29. Rovithis, E.; Makra, K.; Kirtas, E.; Manesis, C.; Bliziotis, D.; Konstantinidou, K. Field Monitoring of Strong Ground Motion in Urban Areas: The Kalochori Accelerometric Network (KAN), Database and Web-GIS Portal. *Earthq. Spectra* **2018**, *34*, 471–501, doi:10.1193/052917EQS098DP.
30. Scibek, J. Multidisciplinary database of permeability of fault zones and surrounding protolith rocks at world-wide sites. *Sci. Data* **2020**, *7*, 1–14, doi:10.1038/s41597-020-0435-5.
31. Di Felice, P.; Spadoni, M. MAHA: A comprehensive system for the storage and visualization of subsoil data for seismic microzonation. *Comput. Geosci.* **2013**, *54*, 113–121, doi:10.1016/j.cageo.2012.11.021.
32. Bard, P.Y.; Gueguen, G.; Wirgin, A. A note on the seismic wavefield radiated from large building structures into soft soils. In *Proceedings of 11th World Conference on Earthquake Engineering*, 1996; Paper N.1838.
33. Tsogka, C.; Wirgin, A. Simulation of seismic response in an idealized city. *Soil Dyn. Earthq. Eng.* **2003**, *23*, 391–402, doi:10.1016/S0267-7261(03)00017-4.
34. Mucciarelli, M.; Masi, A.; Gallipoli, M.R.; Harabaglia, P.; Vona, M.; Ponzio, F.; Dolce, M. Analysis of RC building dynamic response and soil-building resonance based on data recorded during a damaging earthquake (Molise, Italy, 2002). *Bull. Seismol. Soc. Am.* **2004**, *94*, 1943–1953, doi:10.1785/012003186.
35. Mucciarelli, M.; Bianca, M.; Ditommaso, R.; Gallipoli, M.R.; Masi, A.; Milkereit, C.; Parolai, S.; Picozzi, M.; Vona, M. Far field damage on RC buildings: The case study of Navelli during the L'Aquila (Italy) seismic sequence, 2009. *Bull. Earthq. Eng.* **2011**, *9*, 263–283, doi:10.1007/s10518-010-9201-y.
36. Laurenzano, G.; Priolo, E.; Gallipoli, M.R.; Mucciarelli, M.; Ponzio, F.C. Effect of vibrating buildings on free-field motion and on adjacent structures: The Bonefro (Italy) case history. *Bull. Seismol. Soc. Am.* **2010**, *100*, 802–818, doi:10.1785/0120080312.
37. Mucciarelli, M.; Bianca, M.; Ditommaso, R.; Vona, M.; Gallipoli, M.R.; Giocoli, A.; Piscitelli, S.; Rizzo, E.; Picozzi, M. Peculiar earthquake damage on a reinforced concrete building in San Gregorio (L'Aquila, Italy): Site effects or building defects? *Bull. Earthq. Eng.* **2011**, *9*, 825–840, doi:10.1007/s10518-011-9257-3.
38. Piro, A.; de Silva, F.; Parisi, F.; Scotto di Santolo, A.; Silvestri, F. Effects of soil-foundation-structure interaction on fundamental frequency and radiation damping ratio of historical masonry building sub-structures. *Bull. Earthq. Eng.* **2020**, *18*, 1187–1212, doi:10.1007/s10518-019-00748-4.
39. Clouteau, D.; Aubry, D. Modifications of the ground motion in dense urban areas. *J. Comput. Acoust.* **2001**, *9*, 1659–1675, doi:10.1142/S0218396X01001509.
40. Guéguen, P.; Bard, P.Y.; Chávez-García, F.J. Site-city seismic interaction in Mexico City - Like environments: An analytical study. *Bull. Seismol. Soc. Am.* **2002**, *92*, 794–811, doi:10.1785/0120000306.
41. Groby, J.P.; Tsogka, C.; Wirgin, A. Simulation of seismic response in a city-like environment. *Soil Dyn. Earthq. Eng.* **2005**, *25*, 487–504, doi:10.1016/j.soildyn.2004.11.007.
42. Kham, M.; Semblat, J.F.; Bard, P.Y.; Dangla, P. Seismic site-city interaction: Main governing phenomena through simplified numerical models. *Bull. Seismol. Soc. Am.* **2006**, *96*, 1934–1951, doi:10.1785/0120050143.

43. Ghergu, M.; Ionescu, I.R. Structure-soil-structure coupling in seismic excitation and “city effect.” *Int. J. Eng. Sci.* **2009**, *47*, 342–354, doi:10.1016/j.ijengsci.2008.11.005.
44. Padrón, L.A.; Aznárez, J.J.; Maeso, O. Dynamic structure-soil-structure interaction between nearby piled buildings under seismic excitation by BEM-FEM model. *Soil Dyn. Earthq. Eng.* **2009**, *29*, 1084–1096, doi:10.1016/j.soildyn.2009.01.001.
45. Schwan, L.; Boutin, C.; Padrón, L.A.; Dietz, M.S.; Bard, P.-Y.; Taylor, C. Site-city interaction: theoretical, numerical and experimental crossed-analysis. *Geophys. J. Int.* **2016**, *205*, 1006–1031, doi:10.1093/gji/ggw049.
46. Agea-Medina, N.; Kharazian, A.; Molina, S.; Galiana-Merino, J.; Soler-Llorens, J.L.. Fundamental period relationship of RC-buildings in Alicante province (Spain). A first step to soil-structure resonance maps. In *Proceedings of XI International Conference of Structural Dynamics 2020*.
47. Pinzón, L.A.; Pujades, L.G.; Macau, A.; Figueras, S. Increased seismic hazard in Barcelona (Spain) due to soil-building resonance effects. *Soil Dyn. Earthq. Eng.* **2019**, *117*, 245–250, doi:10.1016/j.soildyn.2018.11.022.
48. Tallini, M.; Lo Sardo, L.; Spadi, M. Seismic site characterisation of Red Soil and soil-building resonance effects in L’Aquila downtown (Central Italy). *Bull. Eng. Geol. Environ.* **2020**, *79*, 4021–4034, doi:10.1007/s10064-020-01795-x.
49. Brunn, A.; Weidner, U. Hierarchical Bayesian nets for building extraction using dense digital surface models. *ISPRS J. Photogramm. Remote Sens.* **1998**, *53*, 296–307, doi:10.1016/S0924-2716(98)00012-4.
50. Wu, C. Da; Lung, S.C.C.; Jan, J.F. Development of a 3-D urbanization index using digital terrain models for surface urban heat island effects. *ISPRS J. Photogramm. Remote Sens.* **2013**, *81*, 1–11, doi:10.1016/j.isprsjprs.2013.03.009.
51. Warth, G.; Braun, A.; Bödinger, C.; Hochschild, V.; Bachofer, F. DSM-based identification of changes in highly dynamic urban agglomerations. *Eur. J. Remote Sens.* **2019**, *52*, 322–334, doi:10.1080/22797254.2019.1604083.
52. Fratarcangeli, F.; Murchio, G.; Di Rita, M.; Nascetti, A.; Capaldo, P. Digital surface models from ZiYuan-3 triplet: performance evaluation and accuracy assessment. *Int. J. Remote Sens.* **2016**, *37*, 3505–3531, doi:10.1080/01431161.2016.1192308.
53. Lastilla, L.; Belloni, V.; Ravanello, R.; Crespi, M. DSM Generation from Single and Cross-Sensor Multi-View Satellite Images Using the New Agisoft Metashape: The Case Studies of Trento and Matera (Italy). *Remote Sens.* **2021**, *13*, 593, doi:10.3390/rs13040593.
54. DBGT & CTR | RSDI Available online: <http://rsdi.regione.basilicata.it/dbgt-ctr/> (accessed on Mar 31, 2021).
55. RNC Rilevazione Numeri Civici ed Edifici. - Dataset - OpenData Matera Available online: <http://dati.comune.matera.it/dataset/rnc-rilevazione-numeri-civici-ed-edifici> (accessed on Mar 31, 2021).
56. Italian National Institute of Statistics, ISTAT, 2018. Territorial bases and census variables. (Original name in italian: Basi territoriali e variabili censuarie) Available online: <https://www.istat.it/it/archivio/104317> (accessed on Mar 31, 2021).
57. SESAME Project, 2004. Guidelines for the implementation of the H/V spectral ratio technique on ambient vibrations. In: *Measurements, Processing and Interpretation*, (WP12, Deliverable N. D23.12). http://sesame-fp5.obs.ujf-renoble.fr/Papers/HV_User_Guidelines.pdf.
58. Gallipoli, M.R.; Mucciarelli, M.; Šket-Motnikar, B.; Zupančić, P.; Gosar, A.; Prevolnik, S.; Herak, M.; Stipčević, J.; Herak, D.; Milutinović, Z.; et al. Empirical estimates of dynamic parameters on a large set of European buildings. *Bull. Earthq. Eng.* **2010**, *8*, 593–607, doi:10.1007/s10518-009-9133-6.
59. Albarello, D.; Cesi, C.; Eulilli, V.; Guerrini, F.; Lunedei, E.; Paolucci, E.; Pileggi, D.; Puzzilli, L.M. The contribution of the ambient vibration prospecting in seismic microzoning: An example from the area damaged by the April 6, 2009 L’Aquila (Italy) earthquake. *Boll. di Geofis. Teor. ed Appl.* **2011**, *52*, 513–538, doi:10.4430/bgta0013.
60. Comune di Matera - Piano strutturale comunale Available online: <https://www.comune.matera.it/piano-strutturale-comunale> (accessed on Mar 31, 2021).
61. Ivona; Rinella; Rinella Glocal Tourism and Resilient Cities: The Case of Matera “European Capital of Culture 2019.” *Sustainability* **2019**, *11*, 4118, doi:10.3390/su11154118.
62. Agisoft Metashape Available online: <https://www.agisoft.com/> (accessed on Apr 13, 2021).
63. Nascetti, A. (Division of Geoinformatics, KTH Royal Institute of Technology, Stockholm, Sweden); Crespi, M. (Geodesy and Geomatics Division, DICEA, Sapienza University of Rome, Rome, Italy). Personal communication. **2020**
64. Pavlis, N.K.; Holmes, S.A.; Kenyon, S.C.; Factor, J.K. The development and evaluation of the Earth Gravitational Model 2008 (EGM2008). *J. Geophys. Res. Solid Earth* **2012**, *117*, n/a-n/a, doi:10.1029/2011JB008916.
65. Wessel, B.; Huber, M.; Wohlfart, C.; Marschalk, U.; Kosmann, D.; Roth, A. Accuracy assessment of the global TanDEM-X Digital Elevation Model with GPS data. *ISPRS J. Photogramm. Remote Sens.* **2018**, *139*, 171–182, doi:10.1016/j.isprsjprs.2018.02.017.
66. Bossard, M.; Feranec, J.; Otahel, J.; Steenmans, C. CORINE land cover technical guide-Addendum 2000; 2000;
67. Valensise, G.; Tarabusi, G.; Guidoboni, E.; Ferrari, G. The forgotten vulnerability: A geology- and history-based approach for ranking the seismic risk of earthquake-prone communities of the Italian Apennines. *Int. J. Disaster Risk Reduct.* **2017**, *25*, 289–300, doi:10.1016/j.ijdrr.2017.09.014.
68. Guidoboni, E.; *Disastri e ricostruzioni nella storia d’Italia: l’azzardo sismico in un nodo storico non risolto*. In *Building Back Better: idee e percorsi per la costruzione di comunità resilienti*, 1nd ed.; Carocci editore S.p.A., Roma; Grafiche VD srl: Città di Castello (PG), Italy, 2017; Volume 1, pp. 31–37.
69. decreto ministeriale n. 329 del 6 agosto 2020 | mit Available online: <https://www.mit.gov.it/normativa/decreto-ministeriale-n-329-del-6-agosto-2020> (accessed on Mar 31, 2021).
70. Working Group, S. Guidelines for SEISMIC MICROZONATION; Available online: http://www.protezionecivile.gov.it/httpdocs/cms/attach_extra/GuidelinesForSeismicMicrozonation.pdf (accessed on Mar 31, 2021).